Results from the Search for Ultra-High Energy Neutrinos with ANITA-II

Abigail G. Vieregg for the ANITA Collaboration
Department of Physics and Astronomy, University of California Los Angeles,
475 Portola Plaza, Los Angeles, CA, USA 90095-1547

The ANITA (ANtarctic Impulsive Transient Antenna) experiment is an innovative balloon-borne radio telescope, designed to detect coherent Cherenkov emission from cosmogenic ultra-high energy neutrinos with energy greater than 10^{18} eV. The second flight of the ANITA experiment launched on December 21st, 2008, and collected data for 31 days. This new data set allows for the most sensitive search to date for GZK neutrinos, which offer the exciting possibility of independently revealing the sources of the highest energy cosmic rays. We discuss the results from the second flight of ANITA, calibration techniques, analysis methods, and background rejection. In a blind analysis, we find two candidate neutrino events on a background (thermal and man-made noise) of 0.97 ± 0.42.

1 Introduction

Ultra-high energy (UHE) neutrino astronomy (above 10^{18} eV) is a new frontier in particle astronomy which promises to open up a window to the distant universe where classical photon and cosmic-ray astronomy is limited. UHE neutrinos may also help reveal the origin of UHE cosmic rays (UHECRs), a longstanding mystery in astrophysics.

UHE neutrinos are ideal messenger particles for astrophysical sources for two reasons. First, neutrinos point directly back to their source, whereas protons and ions suffer from curvature induced by cosmic magnetic fields. Second, neutrinos, unlike high-energy photons ($E > 100$ TeV), propagate through the universe virtually unattenuated, yielding information about very distant sources that would otherwise be unavailable.

A population of neutrinos above 10^{18} eV is a “guaranteed” bi-product of the Greisen Zatsepin Kuzmin (GZK) process, whereby cosmic rays above $10^{19.5}$ eV interact with the CMB within tens of Megaparsecs of the source [1,2]. Via a Delta resonance, the interaction yields a pion and a proton or neutron, and the charged pion decay chain produces UHE neutrinos. A cutoff in the cosmic-ray spectrum at $10^{19.5}$ eV has been observed by both HiRes and Auger, and is consistent with being from the GZK process [3,4]. Observation of neutrinos produced from this cutoff mechanism would reveal important information about the nature and location of cosmic sources.

The Antarctic Impulsive Transient Antenna (ANITA) experiment is a Long Duration Balloon experiment that searches for coherent radio Cherenkov emission from electromagnetic cascades induced by UHE neutrinos interacting with the Antarctic ice. Strong, coherent radio emission from UHE electromagnetic showers within a dielectric was first predicted by Askaryan in the 1960’s [5], and later confirmed in the lab [6,7]. ANITA views the top of the radially-polarized Cherenkov cone for neutrinos which skim across the ice (up-going neutrinos are absorbed in

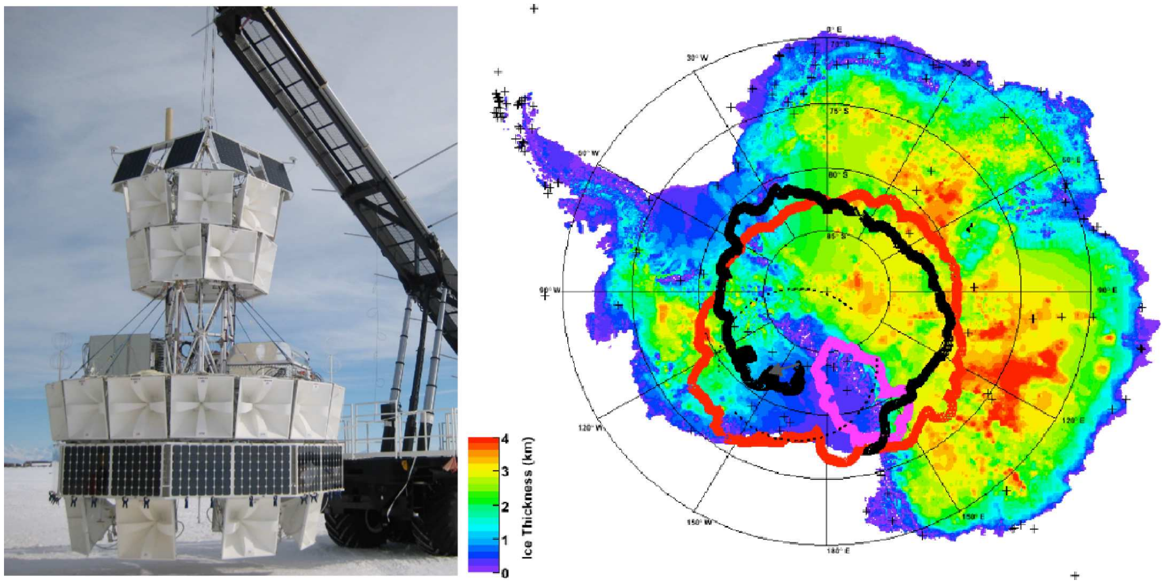

Figure 1: Left: A picture of the ANITA-II payload before launch. Right: The flight path of ANITA-II. Pink is the 1st orbit, red is the 2nd orbit, and black is the 3rd orbit. The map of Antarctica is colored by ice depth.

the Earth). Combined with Fresnel effects at the surface of the ice, this predicts a largely vertically-polarized radio-frequency (RF) signal at the payload from neutrino interactions [5,8,6].

ANITA is also sensitive to radio geosynchrotron emission which reflects off of the Antarctic ice surface from extended air showers of UHECRs. Geosynchrotron emission detected by ANITA is predominantly horizontally polarized because the Earth's magnetic field in Antarctica is mostly vertically polarized, causing the electrons and positrons in the shower to split horizontally, and Fresnel effects at the reflection surface favor the horizontal polarization.

The first flight of ANITA saw no neutrino candidates [9], and set the most constraining limit at the time on the cosmogenic UHE neutrino flux between 10^{18} eV and 10^{21} eV. Further analysis of ANITA-I data revealed 16 observed UHE cosmic rays [10], with energy of order 10^{19} eV.

2 The Second Flight of ANITA

The second flight of ANITA (ANITA-II) launched from Williams Field, Antarctica on December 21, 2008 and landed near Siple Dome after a 31-day flight with 28.5 live days. ANITA-II has 40 quad-ridged horn antennas, is sensitive from 200-1200 MHz, and triggers on fast, broadband signals in the vertical polarization. ANITA-II recorded over $\sim$ 26.7 M events, over 98.5% of which are thermal-noise triggers. Figure 1 shows a picture of the ANITA-II payload and the flight path of ANITA-II.

ANITA-II's sensitivity to cosmogenic neutrinos was improved by about a factor of 4 compared to ANITA-I. Major improvements to the payload included a reduction in front-end system noise temperature, the addition of 8 antennas to the previous total of 32, and the optimization of the trigger for vertically-polarized, broadband impulses. ANITA-II achieved a significant improvement in live time with a flight over deeper ice and the ability to exclude man-made noise from the trigger when in view of strong sources of noise.

3 Data Analysis

The analysis described here is reported in Reference [11] and described in detail in Reference [12]. We performed a blind analysis on the data using two independent methods of blinding. We implemented the "hidden signal box" method, setting all analysis cuts and estimating the background based on sidebands before opening the hidden signal box. The hidden signal region is single, isolated plane-wave events. We also inserted an unknown number of neutrino-like ground-to-payload calibration events randomly throughout the flight and identified inserted events only after the hidden signal box was opened.

For each event, we create an interferometric image in each polarization by cross-correlating waveforms from neighboring antennas and summing the total normalized cross-correlation value for each elevation and azimuth. We construct a "coherently summed" waveform given the direction of the largest peak in either map using the antennas that are closest to that peak. The analysis pointing resolution, determined using ground-to-payload calibration impulses, is $0.2° - 0.4°$ in elevation and $0.5° - 1.1°$ in azimuth, depending on the signal-to-noise ratio (SNR) of the event.

Table 1: Event totals vs. analysis cuts and estimated signal efficiencies for ESS spectral shape [13].

Cut requirement	Passed		Efficiency
	Vpol	HPol	
Hardware-Triggered Events	$\sim$ 26.7M		-
(1) Quality Events	$\sim$ 21.2M		1.00
(2) Reconstructed Events	320,722		0.96
(3) Not Traverses and Aircraft	314,358		1.00
(4) Isolated Singles	7	4	0.64
(5) Not Misreconstructions	5	3	1.00
(6) Not of Payload Origin	2	3	1.00
Total Efficiency			0.61

Table 1 shows the number of events cut and the efficiency of each set of cuts in the analysis. There are two sources of background that must be separated from the signal region. The left panel of Figure 2 shows the reconstructed direction of all 21.2 M Quality Events, and the color of each bin is the average value of the peak of the interferometric map for events which fall in that bin. The blue background is consistent with thermal-noise triggers, and can easily be rejected to a level of 2.5×10^{-8} with a set of cuts on the peak value of the interferometric map and the peak envelope of the coherently summed waveform. An expected background of 0.50 ± 0.23 thermal events passes these reconstruction cuts.

The bright spots in the left panel of Figure 2 are consistent with clusters of man-made noise, which remain after reconstruction cuts are implemented. The right panel of Figure 2 shows all of the 314,358 Reconstructed Events which also are not associated with Traverses and Aircraft tracks and are not in the hidden signal box. Events which remain at this stage are clustered with other events which remain, known places of human activity (camps), and bright spots on the left panel of Figure 2 (Hot Spots). The right panel of Figure 2 shows the clusters of events with different marker colors and styles; camps are shown in red and Hot Spots are black.

Any remaining unclustered events are deemed Isolated Events, and remain in the hidden box. The isolation requirement lowers acceptance since each event, camp, and Hot Spot excludes a region around it from the analysis. We used seven largely independent methods to estimate that the anthropogenic background remaining after our clustering cuts is 0.65 ± 0.39 vertically polarized (VPol) events and 0.25 ± 0.19 horizontally polarized (HPol) events.

The polarization angle of remaining events is then calculated using Stokes parameters, and the event is assigned to be HPol ($< 40°$), VPol ($> 50°$), or sideband ($40° - 50°$). There were no events remaining in the sideband. Two final cuts are applied by hand. Any event that has a high probability of being a Misreconstruction is removed by hand, *e.g.* we remove any event that clearly peaked at a sidelobe of the pattern in the interferometric image. Also, any event

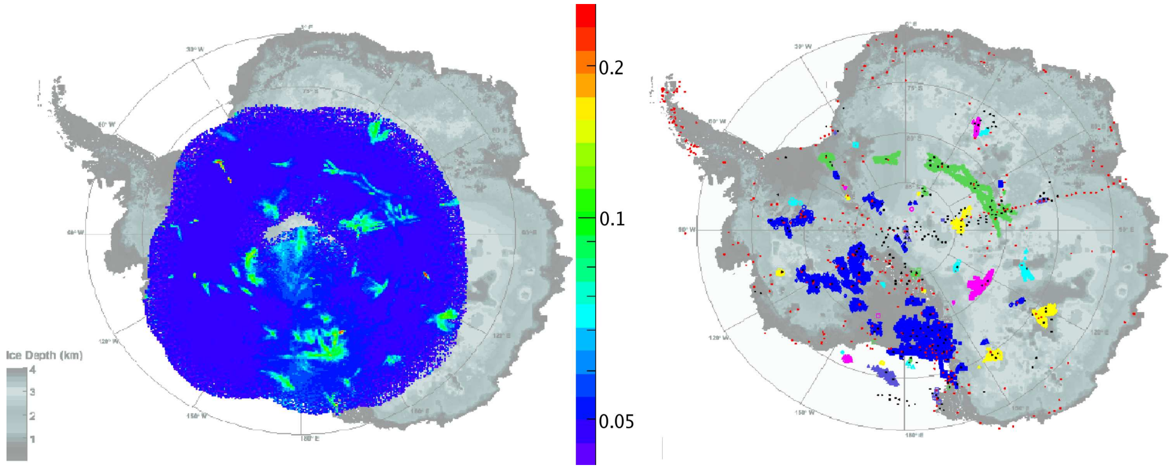

Figure 2: Left: An RF image of Antarctica, seen with ANITA-II. The best direction for all 21.2 M quality events is shown, with one entry per event weighted by the peak value of the interferometric image and each bin normalized by the total number of events which fall in that bin. Right: All 320,722 ANITA-II events which pass thermal-noise (reconstruction) cuts and are not in the hidden signal region shown with locations of known camps (red points) and locations of Hot Spots (black points).

which is clearly of Payload Origin and leaked through the initial quality cuts is also removed by hand; these are also easy to identify.

Upon opening the blind box, we first examine what happened to the 12 inserted neutrino-like events. Of the 12 inserted events, 11 were unique events with one duplicate event. Of the 11 unique events, 8 were Reconstructed Events, consistent with the calculated reconstruction analysis efficiency for such low-SNR events.

4 Results

After all cuts are applied, two events remain in the VPol channel, and three in the HPol channel. After clustering cuts, the thermal noise background reduces to 0.32 ± 0.15 in each channel. The total background is 0.97 ± 0.42 events in the VPol channel, and 0.67 ± 0.24 events in the HPol channel. The left panel of Figure 3 shows the reconstructed locations of the remaining events on the Antarctic continent (blue squares), along with camps (red points), locations of low-level RF noise (black points), and the payload position at the time of detection (black squares), connected to the event location with a line.

All three HPol events show characteristics which identify them as geo-synchrotron radio emission from UHECR air showers, reflecting from the ice surface (including sea ice), as described in the ANITA-I results[10]. While ANITA-I saw 16 such events, the much smaller number of HPol events seen in ANITA-II is due to the change of the trigger to favor VPol events to maximize neutrino sensitivity.

In Figure 3 we show some of the characteristics of the two VPol neutrino candidates, including the waveforms, frequency spectra, and interferometric maps. Event 8381355 has been filtered using the adaptive filter developed for the analysis and is highly impulsive, with a nearly flat radio spectrum. Event 16014510 shows a central impulse with some additional distributed signal within 10-15 ns of the peak, and a frequency spectrum peaking near 400 MHz. The event still passes all cuts if the 400 MHz region is filtered by hand. The reconstructed directions are robust, supporting identification as isolated events. The waveforms and frequency spectra are within the range of simulated neutrino events.

We set a limit including systematic errors[14,15], shown in Figure 4, using the 28.5 day livetime, the energy-dependent analysis efficiency, and the average acceptance from the two independent

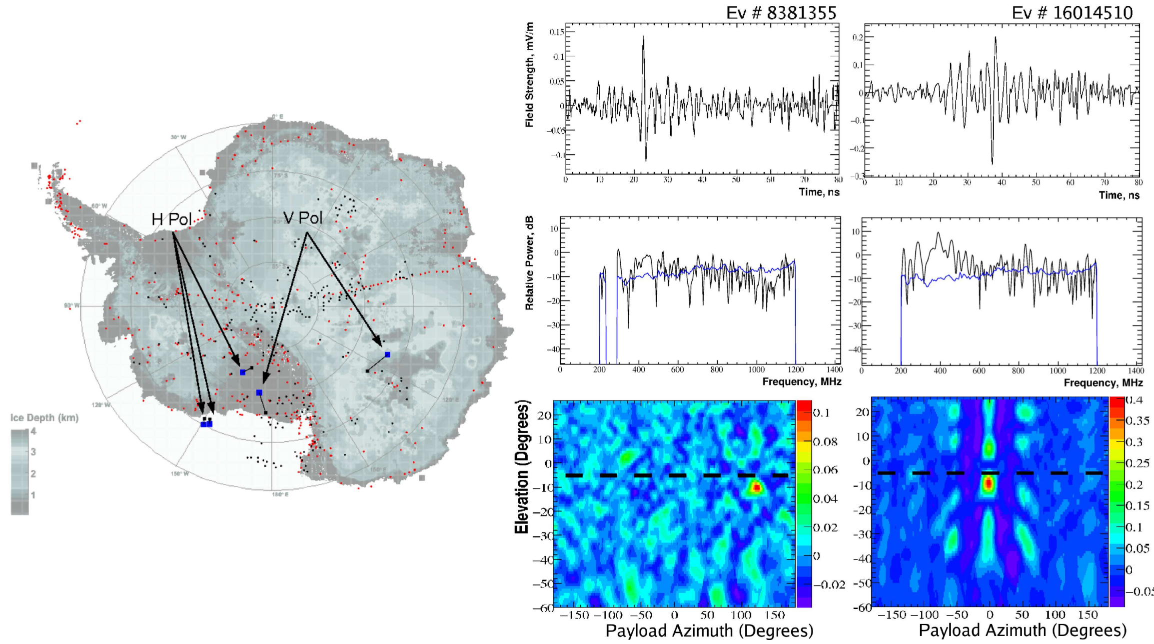

Figure 3: Left: The three cosmic-ray events (HPol) and the two neutrino candidate events (VPol) that remain after opening the hidden signal box. The location of each event (blue squares) and the location of the ANITA payload (black squares) are shown with a connecting line. The locations of known camps (red points) and locations of Hot Spots (black points) are also shown. Top: Waveforms of incident field strength for the two surviving VPol events. Event 8381355 is shown filtered between 235-287 MHz to remove weak CW noise from above the horizon. Middle: Corresponding frequency power spectra. Bottom: Corresponding interferometric maps showing the pulse direction. The dashed line is the horizon.

simulations [16]. The largest systematic error is on the acceptance, which is calculated using two largely-independent Monte Carlo simulations [16]. We take the difference between the two simulations, typically 20%, as a systematic error. The inclusion of systematic errors only worsens the limit by 10%.

5 Discussion

The expected limit from this data in the absence of signal, is about a factor of four more sensitive than ANITA-I [9]. The actual limit, shown in Figure 4, includes our two observed candidates. Because ANITA-II saw more than the expected background, the actual limit is only a factor of two better than ANITA-I even though the discovery potential is four times higher for ANITA-II.

ANITA-II's constraint on cosmogenic neutrino models strongly excludes models with maximally energetic UHECR source spectra which saturate other available bounds[28,23,25]. ANITA-II is now probing several models with strong source evolution spectra that are plausible within current GZK source expectations [23,25,29,27,30], some at $> 90\%$ confidence level. These are the strongest constraints to date on the cosmogenic UHE neutrino flux.

References

1. K. Greisen, Phys. Rev. Lett. 16, 748 (1966).
2. G. Zatzepin and V. Kuzmin, JETP Lett. 4, 78 (1966).
3. R. Abbasi *et al.*, Phys. Rev. Lett. 100, 101101 (2008).
4. J. Abraham *et al.*, Phys. Rev. Lett. 101, 061101 (2008).
5. G. Askaryan, Soviet Physics JETP-USSR 14 (2), 441-443 (1962).

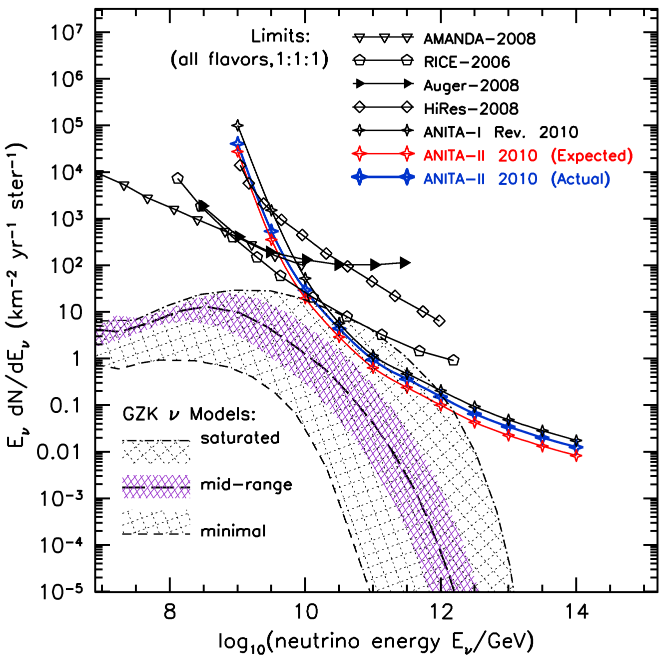

Figure 4: ANITA-II limit for 28.5 days livetime. The red curve is the expected limit before unblinding, based on seeing a number of candidates equal to the background estimate. The blue curve is the actual limit, based on the two surviving candidates. Other limits are from AMANDA,[17] RICE,[18] Auger,[19], HiRes.[20], and a revised limit from ANITA-I[21]. The GZK neutrino model range is determined by a variety of models.[22,13,23,24,25,26,27]

6. D. Saltzberg *et al.*, Phys. Rev. Lett. 86, 2802 (2001).
7. P. Gorham *et al.*, Phys. Rev. Lett. 99, 171101 (2007).
8. J. Alvarez-Muniz and E. Zas, Phys. Lett. B 411, 218-224 (1997).
9. P. Gorham *et al.*, Phys. Rev. Lett. 103, 051103 (2009).
10. S. Hoover *et al.*, Submitted to Phys. Rev. Lett., arXiv:1005.0035 (2010).
11. P. Gorham *et al.*, Submitted to Phys. Rev. D, arXiv:1003.2961 (2010).
12. A. Vieregg, Ph.D. Dissertation, UCLA (2010).
13. R. Engel, D. Seckel, T. Stanev, Phys. Rev. D 64, 093010 (2001).
14. G. Feldman and R. Cousins, Phys. Rev. D 57, 3973 (1998).
15. J. Conrad *et al.*, Phys. Rev. D 67, 012002 (2003).
16. P. Gorham *et al.*, Astropart. Phys. 32, 10-41 (2009).
17. M. Ackermann *et al.*, Ap. J. 675, 1014 (2008).
18. I. Kravchenko, *et al.*, Phys. Rev. D 73, 082002 (2006).
19. J. Abraham *et al.*, Phys. Rev. Lett. 100, 211101 (2008).
20. R. U. Abbassi *et al.*, Ap. J. 684, 790 (2008).
21. S. Hoover, Ph.D. Dissertation, UCLA (2010).
22. R. Protheroe, P. Johnson, Astropart. Phys. 4, 253 (1996).
23. O. Kalashev *et al.*, Phys. Rev. D 66, 063004 (2002).
24. O. Kalashev *et al.*, Phys. Rev. D 65, 103003 (2002).
25. C. Aramo, *et al.*, Astropart. Phys. 23, 65 (2005).
26. M. Ave *et al.*, Astropart. Phys. 23, 19 (2005).
27. V. Barger, P. Huber, D. Marfatia, Phys. Lett. B 642, 333 (2006).
28. S. Yoshida *et al.*, Ap. J. 479, 547 (1997).
29. V. Berezinsky, astro-ph/0509675 (2005).
30. H. Yuksel and M. Kistler, Phys. Rev. D 75, 083004 (2007).